Applied Surface Science 336 (2015) 321–328

Contents lists available at ScienceDirect

Applied Surface Science

journal homepage: www.elsevier.com/locate/apsusc

fs- and ns-laser processing of polydimethylsiloxane (PDMS) elastomer: Comparative study

N.E. Stankova[a,*], P.A. Atanasov[a], N.N. Nedyalkov[a], T.R. Stoyanchov[a], K.N. Kolev[b], E.I. Valova[b], J.S. Georgieva[b], St.A. Armyanov[b], S. Amoruso[c], X. Wang[c], R. Bruzzese[c], K. Grochowska[d], G. Śliwiński[d], K. Baert[e], A. Hubin[e], M.P. Delplancke[f], J. Dille[f]

[a] Institute of Electronics, Bulgarian Academy of Sciences, 72 Tsarigradsko Shose, Sofia 1784, Bulgaria
[b] Rostislaw Kaischew Institute of Physical Chemistry, Bulgarian Academy of Sciences, Acad. G. Bonchev Str., Block 11, Sofia 1113, Bulgaria
[c] CNR-SPIN, Dipartimento di Scienze Fisiche, Universita degli Studi di Napoli Federico II, Complesso Universitario di Monte S. Angelo, Via Cintia, I-80126 Napoli, Italy
[d] Photophysics Department, The Szewalski Institute, Polish Academy of Sciences, 14 Fiszera St., 80-231 Gdańsk, Poland
[e] Vrije Universiteit Brussels, Faculty of Engineering, Research group, SURF "Electrochemical and Surface Engineering", Belgium
[f] Université Libre de Bruxelles, Materials Engineering, Characterization, Synthesis and Recycling (Service 4MAT), Faculté des Sciences Appliquées, 1050 Brussels, Belgium

ARTICLE INFO

Article history:
Received 19 June 2014
Received in revised form
18 December 2014
Accepted 18 December 2014
Available online 29 December 2014

Keywords:
PDMS-elastomer
fs- and ns-laser processing
UV and vis ns- and fs-laser treatment
μ-Raman spectrometry
Metallization
Electroless plating

ABSTRACT

Medical grade polydimethylsiloxane (PDMS) elastomer is a widely used biomaterial as encapsulation and/or as substrate insulator carrier for long term neural implants because of its remarkable properties. Femtosecond (λ = 263 and 527 nm) and nanosecond (266 and 532 nm) laser processing of PDMS-elastomer surface, in air, is investigated. The influence of different processing parameters, including laser wavelength, pulse duration, fluence, scanning speed and overlapping of the subsequent pulses, on the surface activation and the surface morphology are studied. High definition tracks and electrodes are produced. Remarkable alterations of the chemical composition and structural morphology of the ablated traces are observed in comparison with the native material. Raman spectra illustrate well-defined dependence of the chemical composition on the laser fluence, pulse duration, number of pulses and wavelength. An extra peak about ~512–518 cm^{-1}, assigned to crystalline silicon, is observed after ns- or visible fs-laser processing of the surface. In all cases, the intensities of Si—O—Si symmetric stretching at 488 cm^{-1}, Si—CH_3 symmetric rocking at 685 cm^{-1}, Si—C symmetric stretching at 709 cm^{-1}, CH_3 asymmetric rocking + Si—C asymmetric stretching at 787 cm^{-1}, and CH_3 symmetric rocking at 859 cm^{-1}, modes strongly decrease. The laser processed areas are also analyzed by SEM and optical microscopy. Selective Pt or Ni metallization of the laser processed traces is produced successfully via electroless plating. The metallization process is not sensitive with respect to the time interval after the laser treatment. DC resistance is measured to be as low as 0.5 Ω mm^{-1}. Our results show promising prospects with respect to use such a laser-based method for micro- or nano-fabrication of PDMS devices for MEMS and NEMS.

1. Introduction

Silicone-based elastomer polydimethylsiloxane (PDMS) is among the most popular technical polymeric materials due to its advantageous properties: simple and inexpensive fabrication process, mechanical flexibility and stability, high dielectric constant and breakdown field, optical transparency in the ultraviolet (UV)–visible (vis) spectral regions, high biocompatibility and biostability. PDMS is widely used in the fabrication of various micro-electro-mechanical systems (MEMS) and nano-electro-mechanical systems (NEMS) devices such as lab-on-a-chip, waveguides and memory-based devices [1–4], dielectric elastomer actuators [5], as well as in numerous pharmaceutical and medical applications [6–8]. Owing to its remarkable properties, the PDMS-elastomer is also used in biomedicine as encapsulation and/or as substrate insulator carrier for long term neural implants [9,10]. Highly flexible polymeric microelectrode arrays (MEAs) based on PDMS-elastomer scaffold composed by micro-channeled tracks as

* Corresponding author at: Institute of Electronics, Bulgarian Academy of Sciences, 72 Tsarigradsko shosse, blvd., 1784 Sofia, Bulgaria.
Tel.: +359 02 595 872/888 441127.
E-mail address: nestankova@yahoo.com (N.E. Stankova).

http://dx.doi.org/10.1016/j.apsusc.2014.12.121
0169-4332/

Table 1
Summary of the laser processing parameters.

	UV	vis	
fs-laser			
Beam spot at the surface $S(r)$ (cm^2)	0.37×10^{-4}	0.37×10^{-4}	Lens focal distance – 7.5 cm
Fluence range F_L ($J\,cm^{-2}$)	1.1–3.9	1.1–5.4	
Absorbed fluence[a] F ($J\,cm^{-2}$)	0.43–1.52	0.07–0.32	
ns-laser			
Average beam spot at the surface $S(r)$ (cm^2)	2.2×10^{-4}	2.5×10^{-4}	Lens focal distance – 22 cm
Fluence range F_L ($J\,cm^{-2}$)	0.7–4.3	3.0–4.0	
Absorbed fluence[a] F ($J\,cm^{-2}$)	0.27–1.68	0.18–0.24	

[a] It should be emphasized that the given absorbed fluences are valid only for the first laser pulse hitting the material. During the multipulse processing the material absorption increases because of the incubation process.

electrodes are applied as neural interfacing technologies for monitor and/or stimulation of neural activity [11–13]. Elastomeric MEAs can be rolled and flexed, thus offering an improved structural interface with neural tissues. Hence, the modification or structure formation of the PDMS elastomer surface opens an interesting research field for different applications.

UV ns- and fs-laser irradiation of PDMS-elastomer under ambient conditions is an easy and powerful method of micromachining allowing activation and functionalization of the surface without altering its bulk properties [14–22]. NIR (near infrared) fs-laser microstructuring of PDMS polymer is also investigated [3,23,24]. Since laser micromachining is based on the laser direct ablation, it appears as a very suitable and low cost technique for the fabrication of tracks and complex 2D/3D structures with dimensions of several tens of microns or less. It can be effectively applied to a wide range of materials, because of the versatile control of the laser beam parameters. Consequently, this approach allows the numbers of electrodes and pads to be increased by miniaturization of the tracks on the PDMS substrate and thus, to increase the nerve selectivity. After laser processing, selective metallization of the as-processed surface is obtained by immersion of the sample into autocatalytic bath containing metal ions (Ni or Pt). For the metallization step, a quite complicated method has been developed for electroless plating of the polymer materials and applied very soon after the ns-laser treatment [14,25,26].

Laser ablation of polymers is a well established process in industrial applications. However, different mechanisms (photothermal and photochemical) are proposed in terms of the dependence of the dynamics of the etching process on laser fluence, wavelength, pulse length, number of pulses (incubation), and intrinsic properties of the polymer materials [27–33], and details of quantitative understanding are still controversial. However, two general processes originating from the excited electronic state created by UV laser light absorption are distinguished: photochemical decomposition [27,28], resulting in direct bond breaking, and photothermal decomposition [29], due to the vibrational relaxation of the excited states. Some authors declared that both thermal and photochemical mechanisms contribute to the ablation at low laser fluences [27,30,31]. Moreover, defects creation into the material, i.e. “incubation”, is considered as responsible for UV laser ablation of polymers [27–32].

The conception of laser-assisted activation of the silicone PDMS surface is described in details elsewhere [14–16,25], and it is expressed in increasing surface chemical reactivity via photolytic decomposition. Briefly, in spite of the low optical absorption of the PDMS polymer to photons with energy in 5.0–2.3 eV range (248–532 nm wavelength range), UV photons are absorbed selectively and exclusively onto Si—C electron bonds. In fact, optical absorption starts at 3.3 eV (~375 nm) in such complex compounds as PDMS-elastomer. As a result, under laser irradiation, organic radicals are expected to be ejected from the surface, whilst Si—O back-bones (the optical absorption starts at 4.7 eV for this) remain as the sole part of the polymer, but with two unpaired electrons named “dangling bond” materializing the surface chemical activation [14,25].

The aim of this paper is to present new approaches in the processing and characterization of PDMS-elastomer treated by UV and vis emitting ns- and fs-laser and the metallization of the obtained tracks, which could remove some critical issues involved in previous approaches regarding the time interval between laser treatment and metallization for both, ns- and fs-laser processing. Additionally, changes of the chemical status and morphology of the processed PDMS surface using different pulse durations and wavelengths is considered. Second, a direct metallization is applied in order to obtain tracks by electroless plating of Ni or Pt excluding sensibilization and chemical activation usually preceding this process.

2. Experimental

PDMS-elastomer sheets (KCC-corporation, South Korea) (800 μm thick) are irradiated with 2nd HG ($\lambda = 527$ nm) and 4th HG ($\lambda = 263$ nm) of Nd:Glass laser system (pulse duration $\tau \approx 300$ fs and rep rate of 33 Hz), respectively. The material is also processed by 2nd HG ($\lambda = 532$ nm) and 4th HG ($\lambda = 266$ nm) of Q-switched Nd:YAG laser (pulse duration $\tau = 15$ ns and rep rate of 10 Hz). The laser beam is focused perpendicularly to the sample surface using lenses with 7.5 and 22.0 cm focal distance for fs- and ns-laser irradiation, respectively. The data of the laser processing parameters are summarized in Table 1. It is worth noting that the ranges of the absorbed fluences presented in the table are valid only for the first laser pulse hitting the material. The next consecutive pulses interacting with the material cause changes of its optical properties. Despite the low absorption of the native PDMS-elastomer material for wavelengths in the range between 263 and 532 nm with (0.39 for $\lambda = 263$ nm and 0.06 for $\lambda = 532$ nm), the laser treatment with the fluences applied (see Table 1) at the wavelengths indicated above is possible because of an incubation process. The latter occurs as a result from the multipulse processing and enhances the optical absorption of the material. The laser processing is performed in air at ambient temperature in a multiple pulsed regime in order to obtain continuous tracks. The laser line tracks are obtained by overlap (up to 90%) of the adjacent laser beam spots. The samples are mounted on a moving stepper-motor computer-controlled x–y table and shifted with a speed in the interval of 8–76 $\mu m\,s^{-1}$. The number of the consecutive pulses (from 8 to 110) per laser beam spot on the material surface is controlled by the moving speed of the table. Continuous trenches with lengths between 3 and 10 mm and widths between 50 and 150 μm, depending on the laser parameters, are produced.

Before laser treatment the PDMS samples are cleaned by following steps: cleaning in a detergent solution using ultrasound bath; rinsing with deionized water; again cleaning with ethanol

in ultrasound bath; and finally air stream drying. After the laser treatment, the PDMS samples are prepared for metallization by rinsing with deionized water and air stream drying. Cleaning is an important step to avoid quick spontaneous decomposition of the electroless solution. Then, electroless deposition of Pt or Ni is applied to the laser processed tracks. Sensitization by tin and activation by palladium usually preceding the electroless deposition on non-conducting materials are not applied. Hydrazine hydrate is used as reducing agent. The pH of the plating baths is ~12 and the deposition temperatures are 70 °C for Pt and 80 °C for Ni, respectively. The deposition is performed for 25 min in a thermostatic vessel, under rigorous stirring. After metallization, the samples are washed with deionized water and dried. It is worth noting that the Ni metallization is the best and cheaper analog of the classic Pt electroless plating process, based on the hydrazine hydrate reducer. The as described metallization, similar to this presented in brief in [22], is much more simple and not as sensitive with respect to the time interval between laser treatment and metallization as proposed in [25,26].

Different experimental techniques are applied to characterize the PDMS-elastomer, as well as the irradiated and metalized tracks: optical spectrometry (Ocean Optics DH-2000); optical microscopy (Opton, West Germany); scanning electron microscopy (SEM) (Hitachi SU-70 with field emission gun) and SEM/FIB (Lyra/Tescan dual beam system); μ-Raman spectrometry (LabRAM HR Evolution-Horiba Scientific), equipped with 100× magnification objective and laser source operating at λ = 532 nm. Second μ-Raman spectrometer (Invia, Renishaw) using 514 nm excitation wavelength and beam spot on a sample ~5 μm × 5 μm for 100× objective is also applied. The spectral resolution of both Raman systems is ~1 cm^{-1}. The μ-Raman spectra of the laser treated PDMS surface are acquired from five different sections at the bottom of each track and compared to the Raman signals of the native material. Cross-sectional thin foils of composite Ni/PDMS perpendicular to the PDMS surface are prepared using the focused ion beam (FIB) technique applying FEI Quanta 200 3D dual beam. These foils are investigated with a scanning transmission electron microscopy technique (STEM) coupled with facility for selected area electron diffraction (SAED) PHILIPS CM 20 Ultratwin.

3. Results and discussion

As is indicated above, the laser processing is accomplished in a multipulse regime in order to obtain continuous tracks. Optical microscopy technique is used to evaluate continuity and depth of the tracks produced at different conditions. The ablated trenches depths depend on the overlapping of the consecutive pulses applied and also are function of the laser energy density. The ablation depth is evaluated by measuring and averaging of five different points at the bottom of the trench with respect to the non-processed surface. Fig. 1(a) and (b) reports the ablation depth for ns- and fs-laser processing as a function of the pulse numbers at a given fluence. As is seen, for all cases the ablation depth increases almost linearly with the number of pulses applied and have some tendency for saturation. Moreover, the ablation depth obtained in case of ns-laser processing (Fig. 1(a)) is much higher compared to the fs-laser processing (Fig. 1(b)).

The chemical composition of the laser treated PDMS surface is investigated by μ-Raman spectroscopy. The μ-Raman spectra are taken and averaged from five different points at the bottom of each track. Typical μ-Raman spectra of the native PDMS-elastomer material show the following peaks (see Figs. 2 and 3) characterizing the various chemical bonds: 488 cm^{-1} (Si—O—Si symmetric stretching); 685 cm^{-1} (Si—CH_3 symmetric rocking); 709 cm^{-1} (Si—C symmetric stretching); 787 cm^{-1} (CH_3 asymmetric

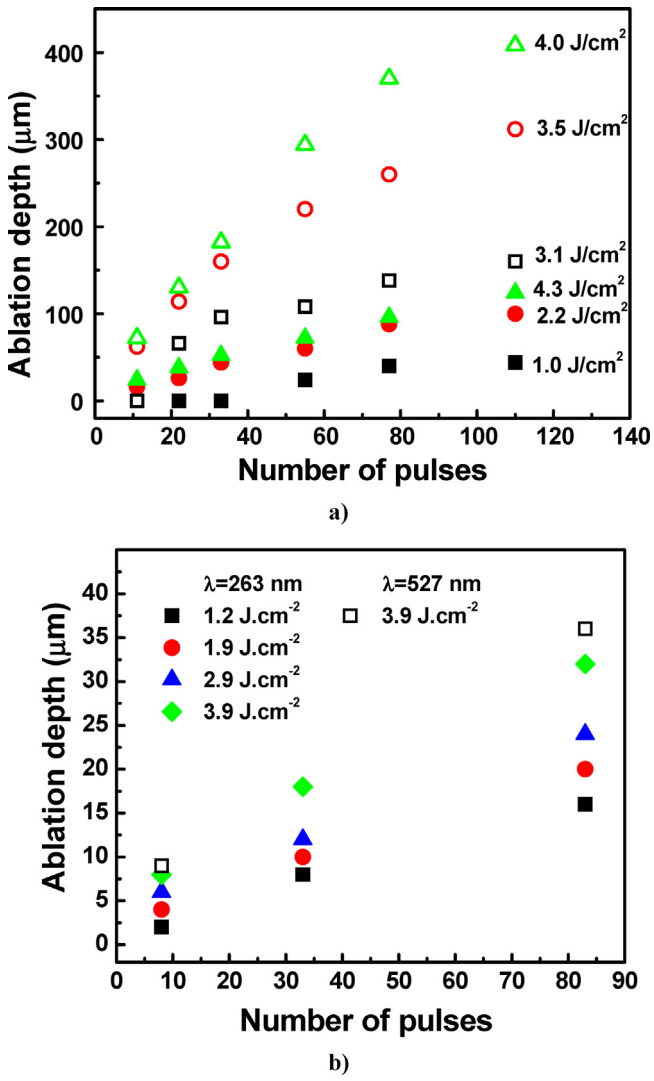

Fig. 1. Ablation depth of the trench produced by the number of subsequent pulses applied at different fluences: (a) ns-laser processing and (b) fs-laser processing. Filled symbols are for UV light and open symbols for vis light, respectively.

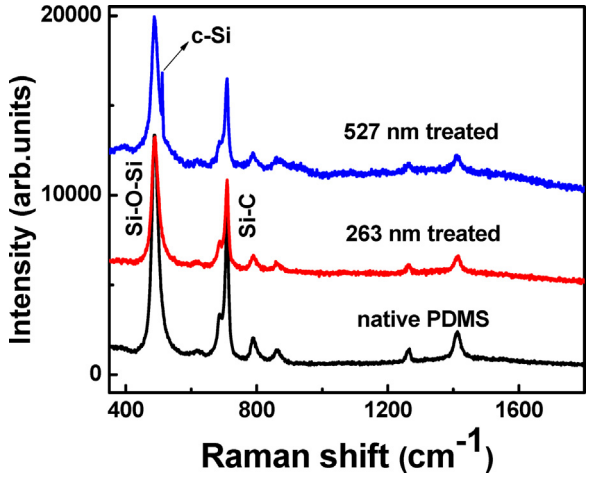

Fig. 2. μ-Raman spectra of native and fs-laser processed PDMS-elastomer. Laser fluence is 3.9 J cm^{-2} in both cases and 83 subsequent laser pulses are applied.

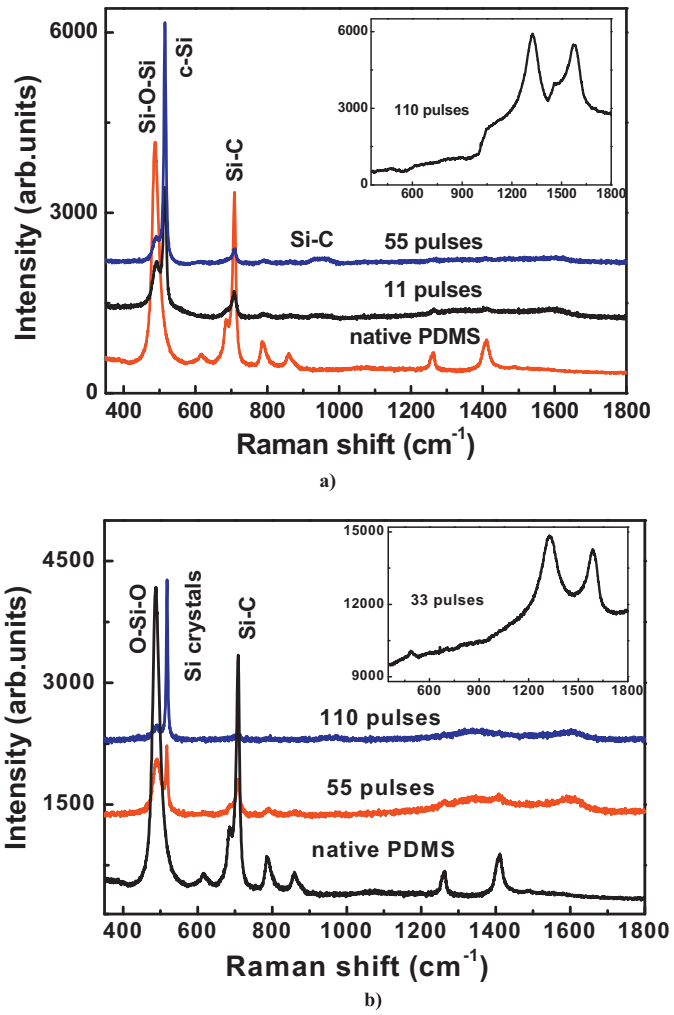

Fig. 3. Changes of the structure of the μ-Raman spectra caused by ns-laser processing: (a) λ = 266 nm and (b) λ = 532 nm. The inset show spectra obtained from some sections of the laser tracks at both wavelengths applied, respectively. The laser fluence applied is 4.3 J cm^{-2} in case of UV light and 4.0 J cm^{-2} in case of vis light, respectively.

rocking + Si—C asymmetric stretching); 859 cm^{-1} (CH_3 symmetric rocking); 1262 cm^{-1} (CH_3 symmetric bending); 1411 cm^{-1} (CH_3 asymmetric bending); 2909 cm^{-1} (CH_3 symmetric stretching); and 2970 cm^{-1} (CH_3 asymmetric stretching) [34].

Fig. 2 reports that the μ-Raman spectra of the fs-laser treated PDMS-elastomer surface differ from the native one, for both 263 nm and 527 nm wavelengths. Local changes in the chemical composition occur at both wavelengths. The intensity of the peaks corresponding to the Si—O—Si, Si—C and methyl stretching bonds gradually decreases with the laser fluence and number of the pulses. It is worth noting that a sharp peak between 512 and 518 cm^{-1}, which can be ascribed to mono and/or polycrystalline or only to monocrystalline silicon (c-Si) [35], appears only in the case of processing with 527 nm. Its intensity increases with the number of the pulses and the laser fluence and is highest at 5.4 J cm^{-2}. According to our knowledge, this is the first observation of c-Si formation by irradiation of PDMS with vis fs pulses. Instead, at 263 nm all the spectral features are similar to the native one, but only a drop of the peaks intensity is observed, as indicated in Ref. [22], which could be explained by depletion of the corresponding chemical bonds.

Fig. 3(a) and (b) represents the μ-Raman spectra of the PDMS-elastomer surface after ns-laser irradiation at 266 nm and 532 nm at the highest laser fluence. The insets in Fig. 3(a) and (b) show μ-Raman spectra acquired in some local laser-treated areas. Significant differences can be observed with respect to the native material surface, demonstrating that ns-laser irradiation induces local chemical transformations of the sample. In spite of the fs-laser treatment areas, the strong and sharp peak between 513 and 518 cm^{-1} occurs in both cases of UV and vis ns-laser processing and is observed in all spectra (i.e. at all processing parameters applied). Its intensity raises with the enhancement of the laser fluence at both irradiation wavelengths, whereas the intensity of the Si—O—Si peak at 488 cm^{-1} decreases. Also, it becomes more dominant with increasing the number of pulses. Therefore, the increase of c-Si band is accompanied by a corresponding reduction of Si—O—Si bonds. The similar Raman spectra measured after UV and vis ns-laser treatment are indicative that at both wavelengths the Si—O bonds are broken, and as a result the formation of the Si clusters is induced. Furthermore, considerable drop of the intensity of the peaks at 685, 709, 787 and 859 cm^{-1} is observed. It clearly reveals that Si—CH_3, Si—C and CH_3 bonds are also broken after the laser treatment, which probably contributes to the formation of Si crystallites as well. Finally, a weak broad Raman band appears between 940 and 960 cm^{-1} after laser treatment with UV (266 nm) light at any number of pulses (Fig. 3(a)), whereas at 532 nm this feature is only observed at the highest number of pulses applied (110 pulses) (Fig. 3(b)). This spectral band can be attributed to the microcrystalline Si—C bond [36]. Obviously, the fs- and ns-laser pulses ablation of the PDMS-elastomer causes similar chemical transformation of its surface, irrespective of the wavelength (i.e. photon energy – UV or vis) applied.

Moreover, after ns-laser processing two new broad peaks are observed in the Raman spectra. It is observed, that in case of UV ns-laser irradiation they appear at 1332 and 1570 cm^{-1} and become dominant at 110 pulses (inset of Fig. 3(a)). Similar trend at 532 nm irradiation is observed, but the peak positions are in the range of 1336–1342 and 1590–1600 cm^{-1}, respectively, when they appear simultaneously with the other Raman peaks (see Fig. 3(b)). However, the μ-Raman spectra obtained from some sections of the laser tracks show only these two peaks (see the inset of Fig. 3(b)). Their appearance is the most expressive feature associated with irradiation with number of pulses larger than 11. It is worth noting, in this case the bands are downshifted at 1332 and 1590 cm^{-1}, respectively. As one can see clearly at both cases (at wavelengths of 266 and 532 nm) the high signal on the peaks tails hinders the other Raman features (insets of Fig. 3(a) and (b)).

According to Refs. [37,38], the broad peaks between 1340 and 1360 cm^{-1} and in the range of 1570 ÷ 1600 cm^{-1} can be assigned to the D band (breathing mode) and G band (stretching mode), respectively, of the sp^2 bonds in amorphous carbon, namely revealing the formation of highly disordered graphite structures, whereas the Raman peak about 1332 cm^{-1} could due to the presence of fraction of sp^3 carbon bonds.

The appearance of the inorganic products (silicon and carbon) in the Raman spectra is certain proof for actual chemical activation of the laser-treated surface. It seems that the surface chemical transformation, i.e. silicone decomposition, is a complex function rather of the laser fluence, pulse duration and the number of the pulses than only of the wavelength. Obviously, as is mentioned above the effective absorption of the PDMS-elastomer is higher enough than that measured at both UV and vis wavelengths used. Therefore, the incubation occurs during the irradiation with every consecutive pulse with respect to the initial laser pulse, which increases the absorption coefficient of the polymer. Most probably, both photothermal and photochemical reactions with ratios could contribute to the ablation mechanism depending on the laser beam parameters (fluence, pulse duration and wavelength) as well as the polymer properties.

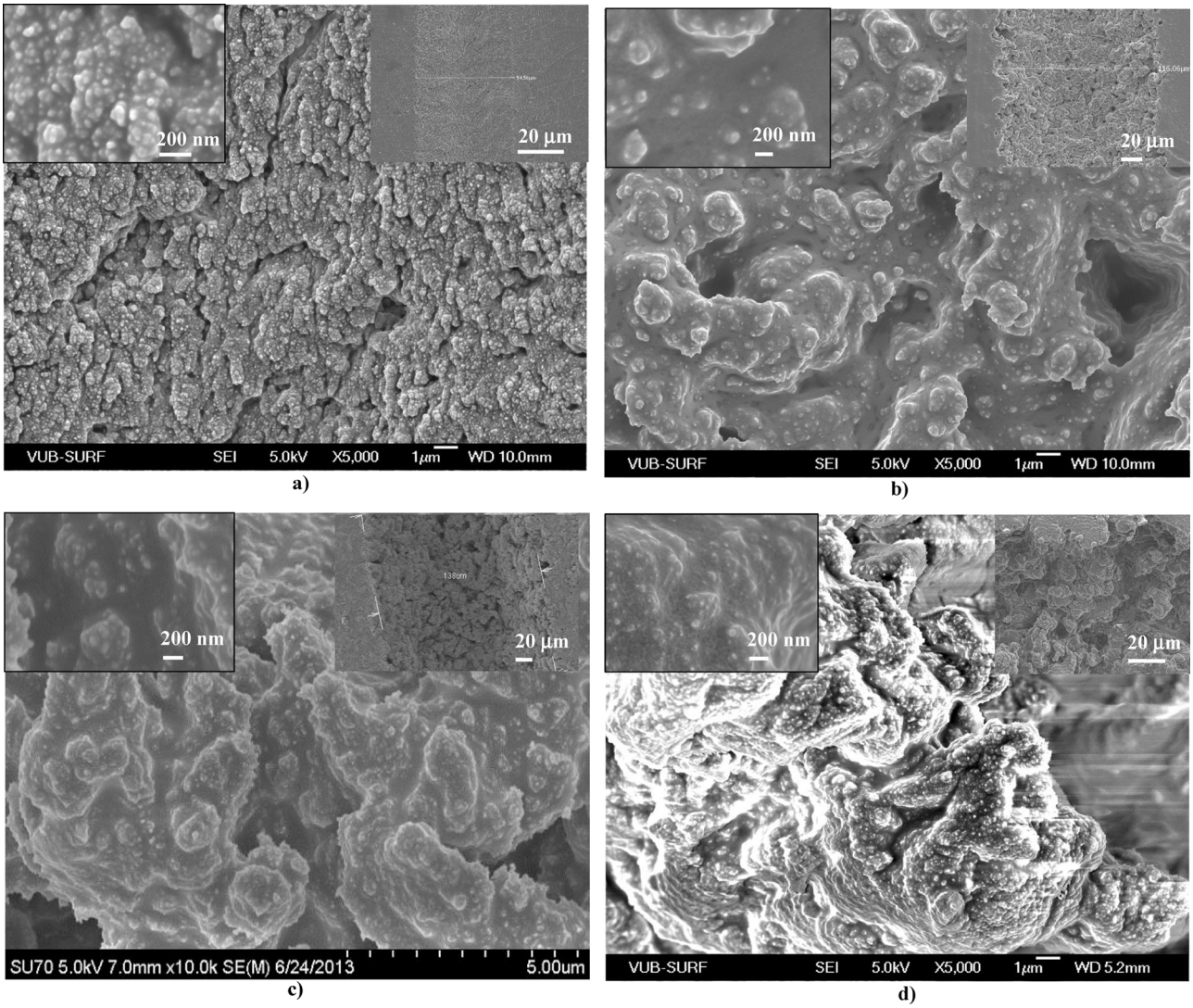

Fig. 4. SEM images indicating PDMS-elastomer surfaces processed by: (a) fs-laser ($\lambda = 263$ nm, fluence 3.9 J cm^{-2}); (b) fs-laser ($\lambda = 527$ nm, fluence 3.9 J cm^{-2}); (c) ns-laser ($\lambda = 266$ nm, fluence 4.3 J cm^{-2}); and (d) ns-laser ($\lambda = 532$ nm, fluence 4.0 J cm^{-2}). The inserts at upper right corners depict part of the tracks areas produced with 83 pulses for fs-laser processing and 77 pulses for ns-laser, respectively. The inserts at the upper left corners show high magnification (200 nm) of the laser processed area with the corresponding laser parameters given above.

Finally, all μ-Raman spectra are measured up to 3200 cm^{-1}. However, they are presented in Figs. 2 and 3 up to 1800 cm^{-1}, since the peaks of the methyl group at 2909 cm^{-1} (CH_3 symmetric stretching) and 2970 cm^{-1} (CH_3 asymmetric stretching) do not express changes in the form, but their intensities only decrease with the fluence or number of pulses increase.

The surface morphology of the laser-processed tracks is studied by SEM and the effects of the various parameters (pulse duration, wavelength, and number of overlapping pulses at the highest fluence) are investigated. Generally, the morphology of all processed areas is characterized by a high roughness. SEM analysis shows broadly similar morphologies for fs- and ns-laser irradiation. As an example, Fig. 4(a)–(d) reports SEM images for UV and vis fs- and ns-laser irradiation, respectively. Additionally, parts of the tracks are exposed as insets at the upper right corners. It is evident that the UV and vis ns- (Fig. 4(c) and (d)) and vis fs-laser (Fig. 4(b)) processed material has very chaotic granular chondrites-like structure with voids, whereas the UV fs-laser treated surface is more regular and uniform. Pores and cavities with different sizes are formed in all cases, but they are much larger for UV and vis ns-laser and vis fs-laser treatment. Also, their concentration and size increase with the number of pulses. Moreover, for both ns- and fs-laser treatment, nm-scale grains can be clearly observed, which origin could due to the inorganic products after the silicone decomposition. Melting and solidification of the material is clearly observed at UV and vis ns- and vis fs-laser treatment independent on the number of pulses applied. Whereas, at UV fs-laser micromachining this trend is weakly expressed and the concentration of the grains is much higher (see the insets at high magnifications of HR SEM images in Fig. 4, insets at the upper left corners).

The following step after the laser activation of the polymer surface is the selective metal deposition by immersion of the sample in autocatalytic bath. It should note the well-known fact, that the silicon and the carbon both induce successful electroless metal (Ni or Pt) plating. Pt and Ni metalized tracks are also characterized using SEM. SEM pictures of electroless deposited Ni areas of UV fs- and ns-laser processed samples are presented in Fig. 5(a) and (b), respectively. It is seen that the metal coats uniformly the laser processed surface. In the case of tracks produced by ns-laser irradiation, Ni crystallizes in "pappus" globules-like structure, whereas for

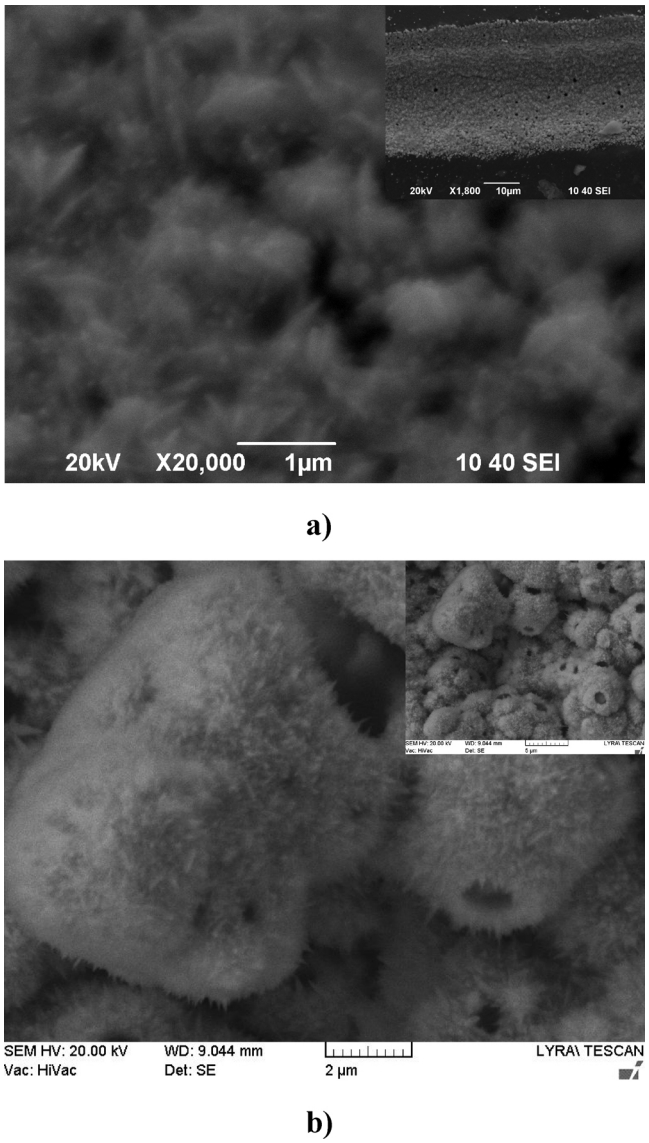

Fig. 5. SEM pictures indicating the Ni metallized tracks by electroless plating after: (a) UV fs-laser processing of PDMS-elastomer, laser energy is 3.9 J cm^{-2} and 83 pulses are applied; (b) UV ns-laser processing of PDMS-elastomer, laser energy is 4.3 J cm^{-2} and 77 pulses are applied.

fs-laser tracks are coated with fine needle-like Ni crystals. It should be underlined that according to our knowledge, first successful metallization of vis (wavelength of 527 and 532 nm) laser-treated PDMS-elastomer is performed.

The best way to demonstrate the ability to activate PDMS for a direct metallization with visible laser is to present a cross section of the composite Ni/PDMS – Fig. 6. The interface of PDMS-Ni is seen there: Fig. 6(a) both components have different density and due to this one can see the complicate interface profile generated by the laser treatment. The complex interface morphology favors the good nickel adhesion through the so called "button up" effect. The details of the electroless deposited Ni crystalline structure, typical for a metal coating are demonstrated in Fig. 6(b) as well as its SAED in Fig. 6(c).

DC resistance of Pt and Ni tracks is measured, resulting always between 0.5 and 15 Ω/mm. It should be noted that the metallized polymer sample keeps most of its original flexability, which is important property for neural probe applications.

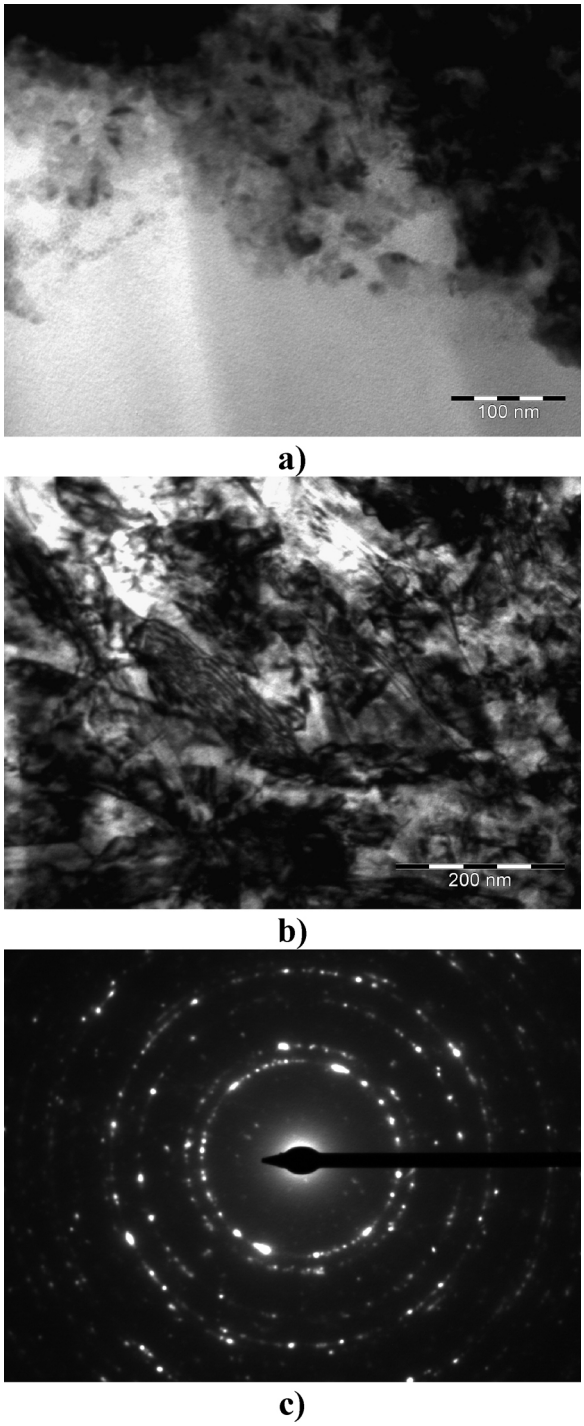

Fig. 6. FIB TEM images of the cross section of Ni metalized tracks produced by vis fs-laser at laser energy 3.9 J cm^{-2}: (a) the interface Ni-PDMS; (b) bright field image in Ni area; (c) SAED: Ni crystalline structure.

Finally, the influence of the time interval between the PDMS-elastomer irradiation and the electroless deposition is investigated. We observed that this time lag is not a very critical parameter for the successful metallization of the samples with Ni and Pt as it is pointed out in Refs. [25,26]. In fact, as is shown before in case of fs UV laser treatment only [22], successful metallization of the tracks is achieved even after 4 or more weeks after surface laser processing. This result represents an important advantage of the simple procedure used here, which is relevant from the point of view of a practical use of this technology.

4. Conclusions

The results of the investigation of the surface modifications due to micromachining of PDMS-elastomer by fs- (λ = 263 and 527 nm) and ns-laser (266 and 532 nm) irradiation can be summarized as follows: It is found by μ-Raman characterization that chemical activation by decomposition of the silicone is induced after fs- and ns-laser treatment of the surface, which results in strong decrease of the intensities of the Si—O—Si stretching mode at 488 cm^{-1}, Si—CH_3 symmetric rocking at 685 cm^{-1}, Si—C symmetric stretching at 709 cm^{-1}, CH_3 asymmetric rocking + Si—C asymmetric stretching at 787 cm^{-1}, CH_3 symmetric rocking at 859 cm^{-1} CH_3, CH_3 symmetric at 2909 cm^{-1} and CH_3 asymmetric at 2970 cm^{-1} stretching modes. Several different important features are evidenced, such as: (i) Si crystallites are formed into tracks fabricated by ns-laser ablation at both wavelengths (266 and 532 nm), while in the fs case, this only happens for processing at 527 nm; (ii) during the ns-laser activation of the surface amorphous carbon containing sp^2 and sp^3 sites is formed. As the Si crystalline peak becomes more prominent, the intensity of the carbon bands decreases accordingly. The local chemical transformations are a complex function rather of the laser fluence, pulse duration and the number of the pulses (incubation) than only of the wavelength.

Optical microscopy and SEM revealed the following peculiarities: (i) all processed areas show a high-roughness morphology with the presence of pores and cavities of different sizes, which are much larger in the case of ns- and vis fs-laser treatment; (ii) the ns- and vis fs-laser processed material presents a more chaotic structure, whereas the UV fs-laser treated surface is more regular and uniform; (iii) all laser treated samples show the presence of nanometer-scale grains. The increase of the number of overlapping pulses leads to more pronounced structure seemingly due to melting and solidification of the material.

The laser treatment is followed by a successful electroless deposition of Ni or Pt in the tracks, excluding sensibilization and chemical activation usually preceding this process. In this way a selective metallization is performed without application of masks or external templates. It is worth noting, that this process is successfully accomplished after vis laser treatment. Strikingly, it is found that when both fs- or ns-laser are applied, the time interval between laser treatment and metallization is not a critical process parameter.

Our results show promising prospects with respect to apply such methods of laser-based micro- or nano-fabrication and electroless metal plating of PDMS-elastomer devices used as MEMS, NEMS and MEAs, having applications for implanted neural interfacing technologies for monitor and/or stimulation of neural activity.

Acknowledgements

The authors would like to acknowledge the support of the following bilateral joint projects between Bulgarian Academy of Sciences (BAS) and foreign research institutions: BAS/CNR (Italy) – project “Femtosecond and nanosecond laser ablation-assisted fabrication of metal and metal-oxides nanostructures”; BAS/Polish Academy of Sciences (Poland) – project “Fabrication and characterization of noble metal nanoparticles arrays”; BAS/Fonds Wetenschappelijk Onderzoek (Belgium) – project “Electrochemical preparation, modification and characterization of nanostructured materials”; and BAS/Wallonie-Bruxelles International – project “New methods for polymer pretreatment for the deposition of nanostructured coatings”. Financial support of the BNSF under the project entitled “New advanced method for processing nanocomposite materials for creation of microsystems for medical and high-tech applications” is acknowledged.

References

[1] A. Asgar, S. Bhagat, P. Jothimuthu, I. Papautsky, Photodefinable polydimethylsiloxane (PDMS) for rapid lab-on-a-chip prototyping, Lab Chip 7 (2007) 1192–1197.
[2] L. Narayana, D. Kallepalli, V.R. Soma, N.R. Desai, Femtosecond-laser direct writing in polymers and potential applications in microfluidics and memory devices, Opt. Eng. 51 (7) (2012) 073402.
[3] K.L.N. Deepak, S. Venugopal Rao, D. Narayana Rao, Femtosecond laser-fabricated microstructures in bulk poly(methylmethacrylate) and poly(dimethylsiloxane) at 800 nm towards lab-on-a-chip applications, Pramana – J. Phys. 75 (6) (2010) 1221–1232.
[4] K. Liu, Z. Nickolov, J. Oh, H. Moses Noh, KrF excimer laser micromachining of MEMS materials: characterization and applications, J. Micromech. Microeng. 22 (1) (2012) 015012.
[5] S. Rosset, H.R. Shea, Flexible and stretchable electrodes for dielectric elastomer actuators, Appl. Phys. A: Mater. Sci. Process. 110 (2013) 281–307.
[6] A. Colas, J. Cutis, in: B.D. Ratner, A.S. Hoffman, F.J. Schoen, J.E. Lemans (Eds.), Biomaterials Science – An Introduction to Materials in Medicine, vols. 2.3 and 7.19, Elsevier, London, UK, 2004, pp. 80–86, 697–707.
[7] K. Gao, L. Li, L. He, K. Hinkle, Y. Wu, J. Ma, L. Chang, X. Zhao, D.G. Perez, S. Eckardt, J. McLaughlin, B. Liu, D.F. Farson, L.J. Lee, Design of a microchannel-nanochannel-microchannel array based nanoelectroporation system for precise gene transfection, Small 10 (5) (2014) 1015–1023.
[8] H. Huang, Z. Guo, Ultrashort pulsed laser ablation and stripping of freeze-dried dermis, Lasers Med. Sci. 25 (4) (2010) 517.
[9] C. Hassler, T. Boretius, T. Stieglitz1, Polymers for neural implants, J. Polym. Sci. B: Polym. Phys. 49 (1) (2011) 18–33.
[10] G.S. Liang Guo, Guvanasen, C. Xi Liu, T.R. Tuthill, S.P.D. Nichols, A PDMS-based integrated stretchable microelectrode array (is MEA) for neural and muscular surface interfacing, IEEE Trans. Biomed. Circuits Syst. 7 (1) (2013) 1–10.
[11] Mohamad HajjHassan, Vamsy Chodavarapu, Sam Musallam, NeuroMEMS: neural probe microtechnologies, Sensors 8 (10) (2008) 6704–6726.
[12] S. Lacour, S. Benmerah, E. Tarte, J. Fitz Gerald, J. Serra, S. McMahon, J. Fawcett, O. Graudejus, Z. Yu, B. Morrison, Flexible and stretchable micro-electrodes for in vitro and in vivo neural interfaces, Med. Biol. Eng. Comput. 48 (10) (2010) 945–954.
[13] M. Schuettler, S. Stiess, B.V. King, G.J. Suaning, Fabrication of implantable microelectrode arrays by laser cutting of silicone rubber and platinum foil, J. Neural Eng. 2 (1) (2005) S121.
[14] L.D. Laude, K. Kolev, Cl. Dicara, C. Dupas-Bruzek, Laser metallization for microelectronics and bio-applications, Proc. SPIE 4977 (2003) 578–586.
[15] L.D. Laude, C. Cochrane, Cl. Dicara, C. Dupas-Bruzek, K. Kolev, Excimer laser decomposition of silicone, Nucl. Instrum. Methods Phys. Res. B 208 (2003) 314–319.
[16] Cl. Dicara, T. Robert, K. Kolev, C. Dupas-Bruzek, L.D. Laude, Excimer laser processing of silicone rubber: from understanding the process to applications, Proc. SPIE 5147 (2003) 255–265.
[17] V.-M. Graubner, O. Nuyken, Th. Lippert, A. Wokaun, S. Lazare, L. Servant, Local chemical transformations in poly(dimethylsiloxane) by irradiation with 248 and 266 nm, Appl. Surf. Sci. 252 (13) (2006) 4781–4785.
[18] K. Rubahn, J. Ihlemann, G. Jakopic, A.C. Simonsen, H.-G. Rubahn, UV laser-induced grating formation in PDMS thin films, Appl. Phys. A 79 (2004) 1715–1719.
[19] C. Dupas-Bruzek, O. Robbe, A. Addad, S. Turrell, D. Derozier, Transformation of medical grade silicone rubber under Nd:YAG and excimer laser irradiation: first step towards a new miniaturized nerve electrode fabrication process, Appl. Surf. Sci. 255 (21) (2009) 8715–8721.
[20] S. van Pelt, A. Frijns, R. Mandamparambil, J. den Toonder, Local wettability tuning with laser ablation redeposits on PDMS, Appl. Surf. Sci. 303 (2014) 456–464.
[21] H. Huang, Yang Lih-Mei, J. Liu, Nanofabrication with UV femtosecond fiber laser, abstract number: 227, in: Natotech Conference & Expo 2012, June 18–21, Santa Clara, CA, USA, 2012.
[22] P.A. Atanasov, N.N. Nedyalkov, E.I. Valova, Zh.S. Georgieva, St.A. Armyanov, K.N. Kolev, S. Amoruso, X. Wang, R. Bruzzesse, M. Sawczak, G. Sliwinski, Fs-laser processing of polydimethylsiloxane, J. Appl. Phys. 116 (2) (2014) 023104.
[23] S. Darvishi, Th. Cubaud, P. Jon, Longtin, Ultrafast laser machining of tapered microchannels in glass and PDMS, Optics Lasers Eng. 50 (2012) 210–214.
[24] C.L. Sones, I.N. Katis, B. Mills, M. Feinaeugle, A. Mosayyebi, J. Butement, R.W. Eason, Rapid and mask-less laser-processing technique for the fabrication of microstructures in polydimethylsiloxane, Appl. Surf. Sci. 298 (2014) 125–129.
[25] L.D. Laude, EP 1995/0693138 A1, US 1997/5599592 A, US 2008/0305320 A1.
[26] C. Dupas-Bruzek, P. Drean, D. Derozier, Pt metallization of laser transformed medical grade silicone rubber: last step toward a miniaturized nerve electrode fabrication process, J. Appl. Phys. 106 (2009) 074913.
[27] E. Sutcliffe, R. Srinivasan, Dynamics of UV laser ablation of organic polymer surfaces, J. Appl. Phys. 60 (9) (1986) 3315–3322.
[28] R. Srinivasan, B. Braren, K.G. Casey, Nature of incubation pulses in the ultraviolet laser ablation of polymethyl methacrylate, J. Appl. Phys. 68 (4) (1990) 1842–1847.
[29] S.R. Cain, F.C. Burns, C.E. Otis, On single-photon ultraviolet ablation of polymeric materials, J. Appl. Phys. 71 (9) (1992) 4107–4116.
[30] A.D. Zweig, V. Venugopalan, T.F. Deutsch, Stress generated in polyimide by excimer-laser irradiation, J. Appl. Phys. 74 (6) (1993) 4181–4189.

[31] V. Srinivasan, M.A. Smrtic, S.V. Badu, Excimer laser etching of polymers, J. Appl. Phys. 59 (11) (1986) 3861–3867.
[32] G.B. Blanchet, P. Cotts, C.R. Fincher, Incubation: subthreshold ablation of poly(methyl methacrylate) and the nature of the decomposition pathways, J. Appl. Phys. 88 (5) (2000) 2975–2978.
[33] Th. Lippert, Laser application of polymers, Adv. Polym. Sci. 168 (2004) 51–246.
[34] S.C. Bae, H. Lee, Z. Lin, S. Granik, Chemical imaging in a surface forces apparatus: confocal Raman spectroscopy of confined poly(dimethylsiloxane), Langmuir 21 (13) (2005) 5685–5688.
[35] C. Palma, M.C. Rossi, C. Sapia, E. Bemporad, Laser-induced crystallization of amorphous silicon-carbon alloys studied by Raman microscopy, Appl. Surf. Sci. 138–139 (1999) 24–28.
[36] Y. Ward, R.J. Young, R.A. Shatwell, A microstructural study of silicon carbide fibres through the use of Raman microscopy, J. Mater. Sci. 39 (2004) 6781.
[37] A.C. Ferrari, Raman spectroscopy of graphene and graphite: disorder, electron–phonon coupling, doping and nonadiabatic effects, Solid State Commun. 143 (2007) 47–57.
[38] A.C. Ferrari, J. Robertson, Origin of the 1150 cm^{-1} Raman mode in nanocrystalline diamond, Phys Rev. B 63 (2001), 121405(R).